

Accepted Manuscript

Synthesis, characterization of 1,2,4-triazole Schiff base derived *3d*-metal complexes: Induces cytotoxicity in HepG2, MCF-7 cell line, BSA binding fluorescence and DFT study

Prateek Tyagi, Monika Tyagi, Swati Agrawal, Sulekh Chandra, Himanshu Ojha, Mallika Pathak

PII: S1386-1425(16)30461-9
DOI: doi: [10.1016/j.saa.2016.08.008](https://doi.org/10.1016/j.saa.2016.08.008)
Reference: SAA 14594

To appear in:

Received date: 21 April 2016
Revised date: 20 July 2016
Accepted date: 7 August 2016

Please cite this article as: Prateek Tyagi, Monika Tyagi, Swati Agrawal, Sulekh Chandra, Himanshu Ojha, Mallika Pathak, Synthesis, characterization of 1,2,4-triazole Schiff base derived *3d*-metal complexes: Induces cytotoxicity in HepG2, MCF-7 cell line, BSA binding fluorescence and DFT study, (2016), doi: [10.1016/j.saa.2016.08.008](https://doi.org/10.1016/j.saa.2016.08.008)

This is a PDF file of an unedited manuscript that has been accepted for publication. As a service to our customers we are providing this early version of the manuscript. The manuscript will undergo copyediting, typesetting, and review of the resulting proof before it is published in its final form. Please note that during the production process errors may be discovered which could affect the content, and all legal disclaimers that apply to the journal pertain.



Synthesis, characterization of 1,2,4-triazole Schiff base derived 3d-metal complexes: Induces cytotoxicity in HepG2, MCF-7 cell line, BSA binding Fluorescence and DFT study

Prateek Tyagi^a, Monika Tyagi^a, Swati Agrawal^b, Sulekh Chandra^{a,*}, Himanshu Ojha^c, Mallika Pathak^d

^a Department of Chemistry, Zakir Husain Delhi College, University of Delhi, JLN-Marg, New Delhi 110002, India

^b Department of Chemistry, Moti Lal Nehru College, Benito Juarez Marg, New Delhi 110021, India

^c Institute of Nuclear Medicine & Allied Sciences, DRDO, Delhi 110054, India

^d Department of Chemistry, Miranda House, University of Delhi, Delhi, 110007, India

*Corresponding author

Tel.: +91-11-22911267; Fax: +91-11-23215906

Email: schandra_00@yahoo.com

Abstract

Two novel Schiff base ligands $\mathbf{H}_2\mathbf{L}^1$ and $\mathbf{H}_2\mathbf{L}^2$ have been synthesized by condensation reaction of amine derivative of 1,2,4-triazole moiety with 2-hydroxy-4-methoxybenzaldehyde. Co(II), Ni(II), Cu(II) and Zn(II) of the synthesized Schiff bases were prepared by using a molar ratio of ligand : metal as 1:1. The structure of the Schiff bases and synthesized metal complexes were established by ¹H NMR, UV-Vis, IR, Mass spectrometry and molar conductivity. The thermal stability of the complexes was study by TGA. Fluorescence quenching mechanism of metal complexes 1–4 show that Zn(II) and Cu(II) complex binds more strongly to BSA. In DFT studies the geometries of Schiff bases and metal complexes were fully optimized with respect to the energy using the 6-31+g(d,p) basis set. The spectral data shows that the ligands behaves as bidentate tridentate. On the basis of the spectral studies, TGA and DFT data an octahedral geometry has been assigned for Co(II), Ni(II), square planar for Cu(II) and tetrahedral for Zn(II) complexes. The anticancer activity were screened against human breast cancer cell line (MCF-7) and human hepatocellular liver

carcinoma cell line (Hep-G2). Result indicates that metal complexes shows increase cytotoxicity in proliferation to cell lines as compared to free ligand.

Key Words: Schiff Base, Co(II), Ni(II),Cu(II) and Zn(II) complexes, DFT, Anticancer activity, BSA binding

ACCEPTED MANUSCRIPT

1. Introduction

There is a considerable increase in the use of metal complexes for cancer treatment after the accidental discovery of the biological activity of platinum complex, cisplatin, in 1965 by Rosenberg [1]. In recent years, many studies associated with metal-based drugs show promising biological activity and are of great interest in chemistry and biology [2]. Literature survey revealed that substituted heterocyclic upon reaction with transition metal salts form complexes that show enhanced physiochemical and pharmacological properties [3–6]. Heteroaromatic moiety on combination with a positive charged metal centre leads to complexes that show well defined geometries, which can easily interact with biomolecules [7].

Transition metal complexes of 1,2,4-triazole substituted moiety have acknowledged considerable interest because of their brilliant coordination potential and diverse pharmacological properties, notable for antibacterial, antifungal, antitumor activities [8–12]. A number of commercially available drugs having 1,2,4-triazole moiety like Vorozole, Letrozole and Anastrozole (**Fig. 1**) are used for the treatment of breast cancer [13]. Other includes, Fluconazole, a very well known antifungal drug and Trazodone is known for their antidepressant properties (**Fig. 1**) [14, 15].

Similarly, the phenolic aldehyde compound like vanillin is very well known. Valen Schiff bases are well known in literature and represents a class of molecule which show extensive biological properties [16–18]. In contrary, a very little work has been published on Schiff base derived from another isomer of vanillin i.e. 2-hydroxy-4-methoxybenzaldehyde [19]. An added advantage of using 2-hydroxy-4-methoxybenzaldehyde over vanillin is the position of –OH group. The –OH group present at the ortho position can easily deprotonate and coordinate with metal centre.

Metals like cobalt, nickel and copper have great affinity for coordination because of their smaller size, higher nuclear charge. To the best of our knowledge no work has been reported on the synthesis of metal complexes of Schiff bases derived from 1,2,4-triazole amine derivatives and 2-hydroxy-4-methoxybenzaldehyde. Two novel Schiff base ligands $\mathbf{H}_2\mathbf{L}^1$ and $\mathbf{H}_2\mathbf{L}^2$ and their metal complexes were synthesized and characterized by ^1H NMR, Mass, IR

and analytical data. The synthesized complexes were screened for their *in vitro* anticancer activity against cell line MCF-7 and HepG2.

Fig. 1.

2. Experimental

2.1 Materials and Methods

All the chemicals were used of Anala R grade and received from Sigma-Aldrich and Fluka. Metal salts were purchased from E. Merck and used as received. MTT (3-(4,5-dimethylthiazole-2-yl)-2,5-diphenyl tetrazolium bromide) and 0.25% trypsin and 0.02% EDTA mixture was purchased from Himedia (India). Fetal bovine serum (FBS) was purchased from Biowest (USA).

2.2 General procedure for the synthesis of Ligands $\mathbf{H_2L^1}$ – $\mathbf{H_2L^2}$

Intermediate **3a-3b** were synthesized from starting compounds (**1a-1b**) (Scheme 1) as per the method reported in literature [13–14]. First the hydrazides (**1a-1b**) were treated with carbon disulphide and potassium hydroxide in absolute ethanol and are converted to their potassium salts (**2a-2b**). On reaction with hydrazine hydrate the potassium salt undergoes ring closure to yield the amine, **3a-3b**. For the synthesis of ligand $\mathbf{H_2L^1}$ equimolar quantity (10 mmol) of **3a** and 2-hydroxy-4-methoxybenzaldehyde (10 mmol) were dissolved in 30 mL of acetic acid. The resultant solution was refluxed for 6 h under constant stirring. After completion of the reaction the solution was poured into crushed ice.

Scheme 1

The separated product was filtered, washed with ice cold water, and recrystallized with a 1:1 solution of DMF & methanol. Similar method was used for the synthesis of ligand $\mathbf{H_2L^2}$. The structure of the synthesized Schiff based were supported by ^1H NMR, IR and Mass spectra.

2.2.1 2-(((3-mercapto-5-(pyridin-4-yl)-4H-1,2,4-triazol-4-yl)imino)methyl)-4-methoxyphenol $\mathbf{H_2L^1}$

Yield: 74(%). Color (pale-yellow). M.p. >260 °C. IR (KBr, cm^{-1}): 1598 $\nu(\text{HC}=\text{N})$, 2704 $\nu(-\text{SH})$, 3230 $\nu(-\text{OH})$. ^1H NMR (DMSO- d_6 , δ , ppm) 3.80 (s, 3H, $-\text{OCH}_3$), 6.82–6.83 (m, 2H, Ar–H), 7.81–7.87 (m, 1H, Ar –H), 8.12 (d, 2H, $J = 6.92$ Hz, Ar–H), 8.75–8.82 (m, 2H,

Ar –H), 9.79 (s, 1H, N=CH), 11.57 (s, 1H, –OH), 14.45 (s, 1H, triazole –SH). Anal. Calcd. for C₁₅H₁₃N₅O₂S (327.36): C: 55.04; H: 4.00; N: 21.39; Found: C: 55.0; H: 4.02; N: 21.35%. Mass spectrum (ESI) [M+H]⁺ = 328.01.

2.2.2 2-(((3-mercapto-5-(pyridin-3-yl)-4H-1,2,4-triazol-4-yl)imino)methyl)-4-methoxyphenol **H₂L²**

Yield: 69(%). Color (yellow). M.p. >260 °C. IR (KBr, cm⁻¹): 1598 ν(HC=N), 2698 ν(–SH), 3213 ν(–OH). ¹H NMR (DMSO-*d*₆, δ, ppm): 3.89 (s, 3H, –OCH₃), 6.72 (d, 1H, *J* = 7.92 Hz, Ar–H), 6.89–6.93 (m, 1H, Ar –H), 7.89–7.93 (m, 2H, Ar–H), 8.73–8.79 (m, 2H, Ar –H), 9.37 (d, 1H, *J* = 7.32 Hz, Ar–H), 9.93 (s, 1H, N=CH), 11.69 (s, 1H, –OH), 14.39 (s, 1H, triazole –SH). Anal. Calcd. for C₁₅H₁₃N₅O₂S (327.36): C: 55.04; H: 4.00; N: 21.39; Found: C: 55.12; H: 3.98; N: 21.36%. Mass spectrum (ESI) [M+H]⁺ = 328.13.

2.3 General procedure for the synthesis of metal complexes 1–8

Schiff base metal(II) complexes (**1–4**) of ligand **H₂L¹** were synthesized from **H₂L¹** (0.34 g, 1 mmol) in (DMF : Methanol in 1:1) (20 mL) with corresponding metal(II) salts {chloride of Co(II) (0.24g, 1mmol), Ni(II) (0.24 g, 1 mmol), Cu(II) (0.17 g, 1 mmol) and Zn(II) (0.14 g, 1 mmol)} in methanol (20 mL) in 1:1 ratio (Scheme 1). The solution was refluxed for 10–16 hrs. The resulting solution was reduced to half volume on a water bath and kept aside overnight. The solid product separated out, which was *vacuum* filtered, washed with cold ethanol, diethyl ether and dried under *vacuum* over anhydrous CaCl₂ (Yield: 58–72%). Similarly, Schiff base metal(II) (**5–8**) complexes of Schiff base **H₂L²** were prepared. Physical, analytical and spectral data of ligands and metal complexes are given in **Table 1**. Attempt to grow the single crystal of the metal complexes was not successful. To have a understanding of the molecular and electronic structure of the synthesized metal complexes, their DFT study is done. The stability of the proposed geometry is also confirmed by the binding energies values.

2.4 Analysis

The carbon and hydrogen were analyzed on Carlo-Erba 1106 elemental analyzer. The nitrogen content of the complexes was determined using Kjeldahl's method. Molar conductance was measured on the ELICO (CM82T) conductivity bridge. ESI-MS spectra were obtained using a VG Biotech Quattro mass spectrometer equipped with an electrospray ionisation source in the mass range of m/z 100 to m/z 1000. IR spectra (CsBr) were recorded on FTIR BX-II spectrophotometer. NMR spectra were recorded with a model Bruker Advance DPX-300 spectrometer operating at 400 MHz using DMSO- d_6 as a solvent and TMS as internal standard. The electronic spectra were recorded in DMSO on Shimadzu UV mini-1240 spectrophotometer. Thermogravimetric analysis (TGA) was carried out in dynamic nitrogen atmosphere (30 ml/min) with a heating rate of 10 °C/min using a Shimadzu TGA-50H thermal analyzer. EPR spectra of the Cu(II) complexes were recorded as polycrystalline sample at room temperature on E4-EPR spectrometer using the DPPH as the g-marker. Fluorescence spectra was recorded on FS920 Edinburgh Instruments, UK, with standard 3.5 ml quartz cell. The excitation source was xenon lamp (450 W) and sample chamber was equipped with peltier accessory.

2.5 DFT Calculations

The theoretical calculations were performed using the 6-31+g(d,p) basis set as incorporated in Gaussian 09W program [20]. The geometries were optimized with respect to energy using the B3LYP three parameter density functional, which includes Becke's gradient exchange correction [21], the Lee, Yang, Parr correlation functional [22] and the Vosko, Wilk, Nusair correlation functional [23].

2.6 In vitro studies (Cell culturing)

The cell lines HepG2 (liver hepatocellular carcinoma) and MCF-7 (human breast adreno carcinoma) were cultured as monolayers and maintained in Dulbecco's modified Eagle medium (DMEM) supplemented with 10% fetal bovine serum (FBS), 2 mM L-glutamine, 100 U/ml penicillin and 100 mg/ml streptomycin in a humidified atmosphere with 5% CO₂ at 37 °C in T-75 flasks and were sub cultured twice a week. For the assays, cells (2×10^3 cells/well in 200 μ l of complete DMEM) were placed in each well of a 96 well flat bottom plate. Cells were allowed to adhere for overnight, and then treated with 5 μ M and 10 μ M concentration of each H_2L^1 , H_2L^2 and metal complexes (1–8) in DMSO for 48 hrs. The cell proliferation of the control (untreated cells) was fixed to 100%. After completion of

incubation period, 20 μl MTT (5mg/ml) was added to each well for 2 hrs. Following which media was removed and 100 μl of DMSO was added to each well in order to solubilize the formazan. The plate was read using the ELISA reader at a wavelength of 540 nm.

3. Results and discussion

3.1 Micro analysis and molar conductance

The synthesized metal(II) complexes are stable in air, microcrystalline solid, partial soluble in hot methanol, soluble in DMF and DMSO and decompose above 260 $^{\circ}\text{C}$. The molar conductance of the metal complexes **1–8** in DMF showed values in range 5.4–11.6 $\text{ohm}^{-1}\text{cm}^2\text{mol}^{-1}$, which indicates that synthesized complexes are non-electrolytes [24]. Physical measurements and analytical data of the ligands and complexes **1–8** are given in **Table 1**.

Table 1

3.2 Mass Spectra

In the ESI mass spectrum of ligand H_2L^1 peak corresponding to $[\text{M}+\text{H}]^+$ ion appear as molecular ion peak at $m/z = 328.01$ amu. The molecular ion peak confirms the proposed formula $[\text{C}_{15}\text{H}_{13}\text{N}_5\text{O}_2\text{S}]^+$, however the base peak of H_2L^1 was observed at m/z 178.01 amu. The peak corresponding to various fragments in H_2L^1 appears at 311.18, 287.97, 281.18, 203.98, 180.81, 179.68, 177.95, 101.98, and 73.99 amu, respectively.

Similarly, for ligand H_2L^2 the molecular ion peak appears at 328.13 amu, while its base peak was observed at m/z value of 178.14. The m/z peak of the metal complexes **1–8** are given in **Table 1**. The mass spectrum of the metal complex **1** is displayed in **Fig. 2** and the mass spectrum of metal complexes **2–8** are given in supplementary data.

Fig. 2

3.3 ^1H NMR Spectra

The ^1H NMR spectra have been recorded for ligands H_2L^1 and H_2L^2 in DMSO. Appearance of important singlet at δ 9.79 ppm, confirms the synthesis of the hybrid coupled Schiff-base ligand HL^1 (**Fig. 3**), was assigned to imine ($\text{CH}=\text{N}$) proton. A set of doublet and multiplet in the region 6.82–8.82 ppm was assigned to the aromatic protons, whereas a weak singlet at 14.45 ppm corresponds to $-\text{SH}$ proton of triazole ring. The proton of the $-\text{OH}$ group appears

as a singlet at 11.57 ppm. Similarly, in the spectrum of the ligand $\mathbf{H}_2\mathbf{L}^2$, the peak corresponding to azomethine ($-\text{HC}=\text{N}$), $-\text{OH}$ and $-\text{SH}$ protons appear at 9.93, 11.69 and 14.39 ppm, respectively.

In ^1H NMR spectrum of Zn(II) complex (**4**) of ligand $\mathbf{H}_2\mathbf{L}^1$ and complex (**8**) of ligand $\mathbf{H}_2\mathbf{L}^2$ a shift of electron density from ligand to metal ion has been observed. The signal for the azomethine proton is slightly deshielded and appeared at δ 10.01–10.12 ppm. This might be due to the donation of electron density from nitrogen to the Zinc ion. Because of this electron transfer from nitrogen to zinc, a coordinate bond is formed between them ($\text{Zn}\leftarrow\text{N}$) [25]. The characteristic signal for the $-\text{SH}$ and $-\text{OH}$ protons disappeared in the NMR of zinc complex, which indicates the deprotonation of $-\text{SH}$ and $-\text{OH}$ protons during complex formation. All other aromatic protons in the NMR spectrum of zinc complex appeared at almost same chemical shift, as they appear in the spectrum on ligand. The signal for coordinated water in appeared as a broad singlet at δ 3.95 and 3.97 ppm, respectively.

Fig. 3

3.4 IR Spectra

In order to understand the binding mode of synthesized ligands to the corresponding metal ions the IR spectra of ligands $\mathbf{H}_2\mathbf{L}^1$, $\mathbf{H}_2\mathbf{L}^2$ and their metal(II) complexes (**1–8**) are discussed. The potential donor sites like azomethine nitrogen ($-\text{C}=\text{N}$), triazole ($-\text{SH}$) and phenol oxygen ($-\text{OH}$), can easily coordinate with metal ions (**Table 2**). Band corresponding to $\nu(\text{C}=\text{O})$ stretching vibrations was not observed in the IR spectra of ligand $\mathbf{H}_2\mathbf{L}^1$. The band at 1598 cm^{-1} was assigned to $\nu(\text{HC}=\text{N})$ linkage confirms the formation of Schiff base. Similarly, band corresponding to $\nu(\text{HC}=\text{N})$ was observed at 1601 cm^{-1} in ligand $\mathbf{H}_2\mathbf{L}^2$ [24]. The particular bands for $\nu(\text{S}-\text{H})$ vibrations was observed at 2704 cm^{-1} for ligand $\mathbf{H}_2\mathbf{L}^1$, while for ligand $\mathbf{H}_2\mathbf{L}^2$ it appeared at 2698 cm^{-1} [27].

In the IR spectra of the metal complexes, it was observed that band corresponding to $\nu(\text{HC}=\text{N})$ group shifts to lower side by $15\text{--}19\text{ cm}^{-1}$, which indicates a bond is formed between azomethine nitrogen and metal ion [28]. The band in the region of $1586\text{--}1579\text{ cm}^{-1}$ in the IR spectra of metal complexes **1–8** corresponds to $\nu(\text{HC}=\text{N})$ group. The same is also supported by the presence of band corresponding to $\nu(\text{M}-\text{N})$ bond in the range of $423\text{--}449\text{ cm}^{-1}$.

No band related to $\nu(\text{S-H})$ stretching vibrations was observed in the IR spectra of metal complexes, which indicates the deprotonation of the thiol group and coordination of thiol sulphur to metal ion [28]. A lower frequency shift due to $\nu(\text{C-S})$ in the IR spectra of metal complexes around $660\text{--}672\text{ cm}^{-1}$, further confirms this. This is supported by the lower frequency shift which appears in the metal complexes. A new band in range of $342\text{--}366\text{ cm}^{-1}$ in far IR spectra was assigned to $\nu(\text{M-S})$ vibrations. The broad band corresponding to $\nu(\text{-OH})$ stretching vibrations, which appeared at 3230 cm^{-1} in H_2L^1 and 3213 cm^{-1} in H_2L^2 disappeared after complex formation, point up the deprotonation of phenol -OH during complex formation. This is further supported by the appearance of new band due to metal-oxygen bond formation in region $510\text{--}534\text{ cm}^{-1}$ [29].

Table 2

Broad band in the region $3290\text{--}3315\text{ cm}^{-1}$ point toward the presence of coordinated water molecules in the complexes **1–8** [29]. This is further supported by the presence of band corresponding to $\nu(\text{-OH})$ rocking and wagging mode of vibrations $765\text{--}793$ and $710\text{--}723\text{ cm}^{-1}$.

The comparison of the IR data of the ligand and the corresponding metal ion enlighten the tridentate nature of the synthesized Schiff base ligands H_2L^1 and H_2L^2 , which coordinates through azomethine nitrogen, thiol sulphur and oxygen of phenol group. Based on above spectral observations, we conclude that both ligands coordinate bidentate tridentately around the Co(II), Ni(II), Cu(II) and Zn(II) centre.

3.5 Conductance and magnetic susceptibility measurements

The molar conductance values of metal complexes were calculated at room temperature taking DMF as a solvent and the results are displayed in **Table 3**. The molar conductance value are generally used to predict the electrolytic or non-electrolytic nature of the metal complexes. The obtained value of molar conductance ($5.4\text{--}11.6\text{ ohm}^{-1}\text{ cm}^2\text{ mol}^{-1}$) for metal complexes **1–8** hint their non-electrolytic behavior. The magnetic moment values of $4.98\text{--}5.03$ B.M. for Co(II) complexes undoubtedly suggest high spin octahedral geometry with three unpaired electron for Co(II) complexes. The magnetic moment value of $2.94\text{--}2.98$ B.M. for Ni(II) complexes corresponds to two unpaired electrons and octahedral geometry [30].

Similarly, Cu(II) complexes show magnetic moment values of 1.81–1.83 B.M., which indicates one unpaired electron.

Table 3

3.6 Electronic spectra

The electronic absorption spectra of the Co(II), Ni(II) and Cu(II) complexes were recorded in DMSO at room temperature and the result are listed in **Table 3**. The electronic spectra of Co(II) complexes two transitions corresponding 10112–10749 cm^{-1} and 19668–19998 cm^{-1} to ${}^4\text{T}_{1g}(\text{F}) \rightarrow {}^4\text{T}_{2g}(\text{F})$ (ν_1); ${}^4\text{T}_{1g}(\text{F}) \rightarrow {}^4\text{T}_{1g}(\text{P})$ (ν_3), ν_2 which is very close to (ν_3) transition is not observed, but it can be calculated [31] by using relation $\nu_2 = \nu_1 + 10Dq$. The ligand field parameters (Dq , B , β , $\beta\%$) have also been calculated for Co(II) complexes by using Band-fitting equations [32]. The Racah parameter (B) is found to be 671–737 cm^{-1} ($< 971 \text{ cm}^{-1}$), suggesting an overlapping of ligand metal orbital's. The nephelauxetic ratio (β) for cobalt complexes is less than one suggesting partial covalency in the metal ligand bond. These ligand field parameters suggest octahedral geometry for Co(II) complexes [32].

The electronic spectral data of Ni(II) complexes showed d-d bands in the region 10,713–11,044, 15,656–16,415 and 24,125–25,675 cm^{-1} , respectively, assigned to the transitions ${}^3\text{A}_{2g}(\text{F}) \rightarrow {}^3\text{T}_{2g}(\text{F})$, ${}^3\text{A}_{2g}(\text{F}) \rightarrow {}^3\text{T}_{1g}(\text{F})$ and ${}^3\text{A}_{2g}(\text{F}) \rightarrow {}^3\text{T}_{1g}(\text{P})$. The position of these bands indicates that the complexes **2** and **6** have octahedral geometry around the Ni(II) centre. The ligand field parameters (Dq , B , β , $\beta\%$) have also been calculated for Ni(II) complexes using the Band-fitting equations. Racah parameters B is less than the free ion value i.e. 1041 cm^{-1} , which indicates covalent character of the metal ligand bond and overlapping of the ligand metal orbitals. The crystal field splitting energy (Dq) value were found to be in the range 1071–1104 cm^{-1} suggested octahedral geometry for Ni(II) complexes. The ratio of the ν_2/ν_1 (~ 1.5) and $\beta\%$ further supported the octahedral geometry around the Ni(II) centre [26,32].

Electronic absorption spectra of the copper complexes **3** and **7** display a transition in the region 18978–20012 cm^{-1} , which can be assigned as the ${}^2\text{B}_{1g} - {}^2\text{A}_{1g}$ transition, revealing that the Cu(II) complexes exist in the square planar geometry [33,34].

3.7 Thermal Analysis

Thermogravimetric study of the synthesized metal complexes was done up to 1000 °C at a heating rate of 10 °C/min in nitrogen atmosphere. Metal complexes **1–4** and **5–8** show similar decomposition pattern as evident from their TGA graphs. Complex **1** ($[\text{Co}(\text{L}^1)(\text{H}_2\text{O})_3]$) show three step decomposition (**Fig. 4**) within temperature range of 140–660 °C. First step corresponds to the loss of three coordinated water molecules (Found 12.34%, calcd. 12.32%) in temperature range of 140–170 °C. The second decomposition step in temperature range 170–390 °C with mass loss of 30.28% (calcd. 30.37%) corresponding to loss of $\text{C}_8\text{H}_7\text{NO}$. A peak corresponding to mass loss of 40.24% (calcd. 40.20%) at 390–660 °C was due to the loss of triazole moiety in the third step and as a final product, it leaves CoO as residue (Found 17.10%, calcd. 17.12%). The thermal decomposition for this complex can be formulated as follows:



Similar behaviour was observed in the TGA curve of metal complexes **2–3**, while the metal complex **4** display two steps dissociation. Typical TGA curve for metal complexes **1–4** is presented in **Fig. 4**. The temperature ranges and percentage mass losses of the decomposition reactions for the metal complexes **1–4** are given in **Table 4** together with evolved moiety and the theoretical percentage mass losses.

fig. 4

Table 4

3.8 EPR spectra

EPR spectra of Cu(II) complexes were recorded at room temperature as polycrystalline sample, on X band at frequency of 9.1 GHz under the magnetic-field strength of 3000G. The analysis of Cu complex (**3**) gives $g_{\parallel} = 2.148$, $g_{\perp} = 2.067$, $g_{\text{av}} = 2.094$ and $G = 2.20$ (**Table 5**). Similarly, the g -tensor values observed for complex **7** are $g_{\parallel} = 2.241$, $g_{\perp} = 2.074$, $g_{\text{av}} = 2.12$ and $G = 3.25$. These g -values have been used to derive the ground state. In square planar complexes, the unpaired electron lies in $d_{x^2-y^2}$ orbital giving ${}^2\text{B}_{1g}$ as the ground state with $g_{\parallel} > g_{\perp} > 2$, while the unpaired electron lies in the d^{z^2} orbital giving ${}^2\text{A}_{1g}$ as the ground state with $g_{\perp} > g_{\parallel} > 2$. In the present cases, the $g_{\parallel} > g_{\perp} > 2$, therefore the unpaired electron is likely to

be in the $d_{x^2-y^2}$ orbital indicates square planar geometry around the copper(II) ion [35]. The possibility of the dimeric form was ruled out as no signal was observed in the spectrum at half field [36]. This is also supported by the magnetic moments of Cu complexes (1.81–1.83 BM) which confirm the mononuclear nature of the complexes.

Orbital reduction factors, K_{\parallel} and K_{\perp} values which are the measure of the spin-orbit coupling constant $\lambda_o = 823 \text{ cm}^{-1}$ for free copper(II) are obtained using the expression reported by Hathaway *et. al.* [37] and Stevens *et. al.* [38]. The K_{\parallel} and K_{\perp} parameters (**Table 5**) are calculated by using the relation $K_{\parallel} = ca \cdot \alpha\beta_1$ and $K_{\perp} = ca \cdot \alpha\beta$, where α , β_1 and β are the coefficients of $d_{x^2-y^2}$, d_{xy} and d_{xz} , d_{yz} orbitals in the MO's to which they contribute; thus α , β_1 and β measures σ -bonding, in-plane π -bonding and out-of-plane π bonding coefficients, respectively. By assuming $\beta_1 = 1$ (since the ligand has no bond pair available on the N atom for bonding with d_{xy}) the values of α and β are calculated for copper(II) complexes. Both values indicate covalent character in metal–ligand bond.

Table 5

3.9 Protein binding studies

Fluorescence quenching during intermolecular interaction is a common phenomenon that occurs due to various processes such as excited-state reactions, molecular rearrangements, energy transfer, ground-state complex formation and collision quenching [39]. The fluorescence spectra of BSA in presence of metal complexes **1–4** has a strong emission band (λ_{em}) at 327 nm due to the tryptophan residues of BSA. The metal complexes **1–4** used in the present study are expected to interact with the tryptophan residue of the BSA. Owe to this, fluorescence quenching experiments were performed with BSA in the presence of different concentrations to assess binding constants for binding of complexes **1–4** with BSA.

The fluorescence quenching experiment of BSA with metal complex **1** (**Fig. 5(a)**) clearly elucidate that on keeping BSA concentration constant and increasing the metal complex concentration from 6.62–33.2 μM , decrease the emission intensity of BSA considerably. The quenching observed may possibly be due to complexation of BSA with complexes [40]. Similar shift in fluorescence spectra of BSA in presence of different concentration of metal complex was reported by Li *et. al.* [41]. The red shift observed was because of increase in polarity of the microenvironment around the tryptophan residues after binding of complex **1**

with BSA. Possibly, it was due to loss of the compact structure of hydrophobic sub domain IIA where tryptophan-214 is placed [42]. Similarly, fluorescence quenching experiment of BSA with metal complex **2** (**Fig. 5(b)**) clearly explain that on keeping BSA concentration constant and increasing the metal complex concentration from 6.62–33.2 μM , decrease the emission intensity of BSA considerably. The maximum intensity of BSA in absence of Ni complex (**2**) was observed at 328 nm and addition of complex **2** with increasing concentration causes a concentration dependent quenching of intrinsic fluorescence of BSA accompanied with a red shift in the maxima from 327 to 334 nm (**Fig. 5(b)**).

In the fluorescence quenching experiment of copper complex (**3**) with BSA, the maximum intensity of BSA in absence of complex (**27**) was observed at 327 nm and addition of complex **27** cause a red shift in the maxima from 327 to 333 nm. (**Fig. 5(c)**). In fluorescence quenching mechanism of zinc complex (**4**), addition of complex **4** quenched the emission intensity of BSA at 336 nm. This quenching in intensity was accompanied with a blue shift from 336 to 324 nm (**Fig. 5(d)**). It has been reported in literature that interaction between some small molecules *viz.* PAAB, vitamin B12 or cyanocobalamin and colchicines with BSA, blue shift of around 5–8.5 nm was observed in the emission spectra [43–45]. The blue spectral shift indicates increase in hydrophobicity and decrease in polarity around the tryptophan residues. Similar result was observed in fluorescence quenching of metal complex **4** with BSA. A blue shift of 12 nm in our result is comparable to blue shift values reported in literature. This suggests that the binding interaction between the complex **4** and BSA result in enhancement of hydrophobicity around the tryptophan residues of BSA.

Fig. 5

To investigate the fluorescence quenching mechanism for metal complexes **1–4** with BSA, the fluorescence data were further analyzed with Stern-Volmer equation.

$$F_0/F = 1 + K_{sv} [Q]$$

Where, F_0 and F are the fluorescence intensities of BSA in the absence and presence of the quencher molecule, K_{sv} is the Stern-Volmer quenching constant and $[Q]$ is the concentration of the quencher metal complex. The Stern-Volmer plots of metal complexes **1–4** with BSA are given in **Fig. 6**.

Fig. 6

The value of bimolecular quenching rate constant (k_q) was obtained according to Equation

$$F_0/F = 1 + K_{sv} [Q] = 1 + k_q \tau_0 [Q]$$

Where, k_q is bimolecular quenching rate constant; τ_0 is the lifetime of BSA in the absence of quencher and K_{sv} is the Stern Volmer constant. The value of τ_0 for BSA has been reported in many studies and was found to be around 10^{-9} s. From the findings of the fluorescence quenching study, the value of k_q for metal complexes 1–4 ($3.50\text{--}3.78 \times 10^{13} \text{ M}^{-1} \text{ s}^{-1}$) was much greater than the maximum scattering collision quenching constant ($2 \times 10^{10} \text{ M}^{-1} \text{ s}^{-1}$) [46,47] which indicates that the probable quenching mechanism is static quenching. The values of K_{sv} and K_q for the metal complexes 1–4 are given in **Table 6**.

Table 6

Number of binding sites can be calculated from fluorescence titration data using the following equation:

$$\log (F_0 - F)/F = \log K_b + n \log [Q]$$

where K_b and n are the binding constant and binding site for metal complexes 1–4. On plotting $\log[F_0/F]$ versus $\log[Q]$ (**Fig. 7**), a linear graph was obtained. The value of K_b and n were calculated from the slopes and intercepts of the linear plots. The binding constant and number of binding sites (n) are given in Table 6. The binding constant (K_b) value indicates Cu and Zn complexes strongly bind to BSA. Again, the value of n is nearly 1 for binding of both complexes to the protein used, which indicates the high affinity binding sites of albumins. The value of n suggested that there were single class of independent binding sites [48]. The corresponding K_b and n values were evaluated from the slopes and intercepts of the linear plots, respectively. The binding constant and number of binding sites (n) are given in **Table 7**.

Fig. 7

Table 7

3.10 Geometry optimization

Geometry Optimization was done using B3LYP functional with 6-31+g(d,p) basis sets as incorporated in the Gaussian 09W programme in gas phase. The fully optimized geometries

of the ligand $\mathbf{H}_2\mathbf{L}^1$ and complexes $\mathbf{1-4}$ are shown in **Fig. 8**. The numbering scheme for ligand $\mathbf{H}_2\mathbf{L}^1$, and complexes $\mathbf{1-4}$ are given in Scheme 2. The values of the bond length and bond angles calculated for metal complex $\mathbf{1}$ shows octahedral geometry around the Co(II) ion (**Table 8**). A slight elongation in bond lengths C_1-N_1 , N_2-C_8 , N_2-C_9 was noted in complexes $\mathbf{1}$ as ligand $\mathbf{H}_2\mathbf{L}^1$ coordinates via azomethine nitrogen. The $-OH$ and $-SH$ group deprotonate and coordinated to Co(II) ion and no appreciable change was noted in bond lengths C_3-O_1 and C_9-S_1 after metal coordination. The C_3-O_1 and C_9-S_1 bond lengths was found to be 1.464 and 1.787 Å, respectively. The four equatorial positions are occupied by azomethine nitrogen, thiol sulphur and two water molecules, while two axial positions are occupied by water molecule and oxygen of phenol group. The bond angles in the coordination sphere of Co(II) complexes are found approximately near to the perpendicular value. The value of bond angle $\angle N_1MO_1$, $\angle S_1MN_1$, $\angle O_1MO_{11}$, $\angle O_1MS_1$ and $\angle O_{11}MO_{12}$ was found to be 85.46, 86.12, 87.23 and 94.12°, respectively. No appreciable change in bond lengths and bond angle was seen in 1,2,4-triazole moiety and benzene ring.

Fig. 8

Scheme 2

Table 8

Metal complex $\mathbf{2}$ having Ni(II) as metal centre display similar behaviour and exist in octahedral environment. The calculated bond lengths and bond angles lie in same range of the calculated bond lengths and bond angles value of complex $\mathbf{1}$. However, complex $\mathbf{3}$ having Cu(II) metal centre shows square planar arrangement around the metal centre. We also try to optimize Cu(II) complex in octahedral arrangement by adding two more water molecule to the metal centre. But the attempt to optimize the complex was failed as the $Cu-S_1$ bond length elongates to 4.2 Å in the final structure, which causes bond to break and the five membered ring of the 1,2,4- moiety flip out of the plane. Thus the square planar geometry for Cu(II) is stable which also correlate our experimental results. A noteworthy point is that after complexation bond length around the metal centres becomes slightly smaller. The bond length C_1-N_1 , N_1-N_2 , N_2-C_8 and N_2-C_9 becomes shorter by ~ 0.1 Å. This clearly predicts stronger complexation between ligand and metal centre. All the bond lengths and bond angles were found to be in their expected range.

Similar results was noted in complex **4** having zinc metal centre. All the computed bond lengths and bond angles are listed in Table 5. To evaluate the extent of complexation and to find the stability order, we have calculated the binding energy of the four complexes and the result found was: (Binding Energy)₃ > (Binding Energy)₄ > (Binding Energy)₁ > (Binding Energy)₂. On the basis of the above discussion following (**Fig. 9**) structures can be proposed for the synthesized complexes.

Fig. 9

3.11 Cell viability determination

The *in vitro* cytotoxicity of the ligand **H₂L¹**, **H₂L²** and metal complexes (**1–8**) on human cell lines HepG2 and MCF-7 was determined by a MTT based assay. The results are expressed as the percentage of cell toxicity with respect to the control and are represented in Table 8. From the MTT assay data, it can be concluded that control shows a toxicity of 0.25–0.50 % on cell line HepG2 and MCF-7. Ligand **H₂L²** i.e. Schiff base derived from nicotinic acid hydrazide display better activity in comparison to Schiff base derived from isonicotinic hydrazide (**H₂L¹**). Ligand **H₂L²** show a cytotoxicity of 10 % and 9% against cell line HepG2 and MCF-7 at concentration of 5 μ M in comparison to 8% and 5% for ligand **H₂L¹**. Also, metal complexes show higher cytotoxicity in comparison to free ligands. Metal complexes **4**, **7** and **8** display cytotoxicity of 13, 20 and 15% against cell line HepG2, whereas 14, 18 and 19% cytotoxicity was revealed against cell line MCF-7. On increasing the concentration from 5 μ M to 10 μ M no appreciable change in cytotoxicity against cell line HepG2 and MCF-7 was observed for ligand **H₂L¹** and **H₂L²**. But at concentration of 10 μ M complexes **3**, **4**, **7** and **8** show a significant increase in % inhibition on cell proliferation on cell line HepG2 (26, 22, 39 and 31%). Similarly, the complexes **3**, **4**, **7** and **8** shows a significant increase in % inhibition on cell proliferation on cell line MCF-7 (22, 19, 30 and 35%). Cu(II) complexes show best cytotoxicity to cancerous cells, followed by Zn(II) complexes and Co(II) complexes. Ni(II) complexes show the least activity. Graphical representation of the anticancer cell line viability of ligand **H₂L¹**, **H₂L²** and their metal complexes **1–8** against cell line Hep G2 and MCF-7 is shown in **Fig. 10** and tabulated in **Table 9**.

Table 9

Fig. 10

4. Conclusion

The newly synthesized Schiff base ligands $\mathbf{H}_2\mathbf{L}^1$, $\mathbf{H}_2\mathbf{L}^2$ coordinates in a tridentate fashion around the metal (II) centre. Based on various physio-chemical techniques, Co(II) and Ni(II) complexes possessed an octahedral geometry, while Cu(II) complexes exist in square planer and Zn(II) form tetrahedral geometry. The presence of coordinated water was confirmed by the TGA and IR data. The reasonable agreement between the theoretical and experimental data reflects to the great extent the suitability of the applied basis set, 6-31+g(d,p) for this type of work and confirms the suggested structure. The result of interaction of metal complexes with BSA reveal that Zn complex (**4**) binds more strongly to BSA, followed by Cu (**3**), Co(**1**) and Ni(**2**). Results of MTT assay revealed all metal complexes show moderate to significant % inhibition on the cell proliferation on cell line HepG2 and MCF-7. Schiff base derived from nicotinic acid hydrazide display better activity in comparison to Schiff base derived from isonicotinic hydrazide. This inhibition on cell proliferation might be due to azomethine (-HC=N-) linkage and/or hetero atoms present in these compounds.

5. Acknowledgements

We thank the Principal, Zakir Husain Delhi College for providing lab facilities. Authors are thankful to DRDO, for financial assistance.

6. References

1. P. Tyagi, P. Gahlot, R. Kakkar, *Polyhedron*, 27 (2008) 3567.
2. R. P. Bakale, G. N. Naik, C. V. Mangannavar, I. S. Muchchandi, I. N. Shcherbakov, C. Frampton, K. B. Gudasi, *Eur. J. Med. Chem.*, 73 (2014) 38.
3. A. Inam, S. M. Siddiqui, T. S. Macedo, D. R. Magalhaes, A. C. Lima Leite, M. B. Soares, A. Azam, *Eur. J. Med. Chem.*, 75 (2014) 67.
4. W. B. Júnior, M. S. Alexandre-Moreira, M. A. Alves, A. Perez-Rebolledo, G. L. Parrilha, E. E. Castellano, O. E. Piro, E. J. Barreiro, L. M. Lima, H. Beraldo, *Molecules*, 16 (2011) 6902.
5. F. A. Muregi, A. Ishih, *Drug Dev. Res.*, 71 (2010) 20.
6. G. G. Mohamed, E. M. Zayed, A. M. M. Hindy, *Spectrochim. Acta A*, 145 (2015) 76.
7. A. Almeida, B.L. Oliveira, J.D.G. Correia, G. Soveral, A. Casini, *Coord. Chem. Rev.*, 257 (2013) 2689.
8. B. S. Holla, B. Veerendra, M. K. Shivananda, B. Poojary, *Eur. J. Med. Chem.*, 38 (2003) 759.
9. S.V. Bhandari, K. G. Bothara, M. K. Raut, A. A. Patil, A. P. Sarkate, V. J. Mokale, *Bioorg. Med. Chem.*, 16 (2008) 1822.
10. K. V. Sujith, J. N. Rao, P. Shtty, B. Kalluraya, *Eur. J. Med. Chem.*, 44 (2009) 3697.
11. T. Propst, W. Vogel, A. Propst, O. Dietze, H. Braunsteiner, *J. Mol. Med.*, 70 (1992) 55.
12. P. Tyagi, S. Chandra, B. S. Saraswat, D. Yadav, *Spectrochim. Acta A*, 145 (2015), 155.
13. G. Capranico, G. Zagotto, M. Palumbo, *Curr. Med. Chem. Anticancer Agents*, 4 (2004) 335.
14. T. Propst, W. Vogel, A. Propst, O. Dietze, H. Braunsteiner, *J. Mol. Med.*, 70 (1992) 55.
15. S.M. Stahl, *CNS Spectr.*, 13 (2008) 1027.
16. A. Torres, A. Garedeu, E. Schmolz, I. Lamprecht, *Thermochim. Acta*, 415 (2004) 107.
17. M. Montanari, A. Andricopulo, C. Montanari, *Thermochim. Acta*, 417 (2004), 283.
18. R. Prabhakaran, A. Geetha, M. Thilagavathi, R. Karvembu, V. Krishnan, H. Bertagnolli, K. Natarajan, *J. Inorg. Biochem.*, 98 (2004) 2131.
19. E. Pahontu, D. C. Ilies, S. Shova, C. Paraschivescu, M. Badea, A. Gulea, T. Roş u, *Molecules*, 20 (2015) 5771.
20. M. J. Frisch, G. W. Trucks, H. B. Schlegel, G. E. Scuseria, M. A. Robb, J. R. Cheeseman,

- G. Scalmani, V. Barone, B. Mennucci, G. A. Petersson, H. Nakatsuji, M. Caricato, X. Li, H.P. Hratchian, A. F. Izmaylov, J. Bloino, G. Zheng, J. L. Sonnenberg, M. Hada, M. Ehara, K. Toyota, R. Fukuda, J. Hasegawa, M. Ishida, T. Nakajima, Y. Honda, O. Kitao, H. Nakai, T. Vreven, J. A. Montgomery, Jr., J. E. Peralta, F. Ogliaro, M. Bearpark, J. J. Heyd, E. Brothers, K. N. Kudin, V. N. Staroverov, R. Kobayashi, J. Normand, K. Raghavachari, A. Rendell, J. C. Burant, S. S. Iyengar, J. Tomasi, M. Cossi, N. Rega, J. M. Millam, M. Klene, J. E. Knox, J. B. Cross, V. Bakken, C. Adamo, J. Jaramillo, R. Gomperts, R. E. Stratmann, O. Yazyev, A. J. Austin, R. Cammi, C. Pomelli, J. W. Ochterski, R. L. Martin, K. Morokuma, V. G. Zakrzewski, G. A. Voth, P. Salvador, J. J. Dannenberg, S. Dapprich, A. D. Daniels, O. Farkas, J. B. Foresman, J. V. Ortiz, J. Cioslowski, D. J. Fox, Gaussian, Inc., Wallingford CT, 2009.
21. A. D. Becke, *Phys. Rev. A*, 38 (1988) 3098.
 22. C. Lee, W. Yang, R. G. Parr, *Phys. Rev. B*, 37 (1988) 785.
 23. S. H. Vosko, L. Wilk, M. Nusair, *Can. J. Chem.*, 58 (1980) 1200.
 24. W. J. Geary, *Coord. Chem. Rev.*, 7 (1971) 81.
 25. K. Singh, M. S. Barwa, P. Tyagi, *Eur. J. Med. Chem.*, 41 (2006) 147.
 26. P. Tyagi, S. Chandra, B. S. Saraswat, D. Sharma, *Spectrochim. Acta A*, 143 (2015) 1.
 27. G. Singh, P. A. Singh, K. Singh, D. P. Singh, R. N. Handa, S. N. Dubey, *Proc. Natl. Acad. Sci. Ind.*, 72A (2002) 87.
 28. P. Tyagi, S. Chandra, B. S. Saraswat, *Spectrochim. Acta A*, 134 (2015) 200.
 29. M. Tyagi, S. Chandra, P. Tyagi, *Spectrochim. Acta A*, 117 (2014) 1.
 30. S. Chandra, S. Bargujar, R. Nirwal, N. yadav, *Spectrochimica Acta A*, 106 (2013) 91.
 31. F. A. Cotton, G. Wilkinson, C. A. Murillo, M. Bochmann, *Advanced Inorganic Chemistry*. 6th edition, John Wiley & Sons Inc. New York (1999).
 32. A. B. P. Lever, *Inorganic Electronic Spectroscopy*, 2nd edition, Elsevier, Amsterdam (1984).
 33. N. N. Greenwood, A. Earnshaw, *Chemistry of the Elements*, 1st edition, Pergamon Press, UK (1983) 1379.
 34. A. H. Osman, M. S. Saleh, M. M. Sanaa, *Synth. React. Inorg. Met. Org. Chem.*, 34, (2004) 1069.
 35. R. K. Ray, G. B. Kaufman, *Inorg. Chim. Acta.*, 173, (1990) 207.
 36. K. K. Narang, J. P. Pandey, V. P. Singh, *Polyhedron*, 13, (1994) 529.
 37. B. J. Hathaway, A. A. G. Tomilinson, *Coord. Chem. Rev.*, 5 (1970) 1.

38. K. W. H. Stevens, *Proc. Roy. Soc. A*, 219 (1953) 542.
39. Y. J. Hu, Y. Liu, L. X. Zhang, *J. Mol. Struct.*, 750, (2005) 174.
40. S. Saha, R. Majumdar, M. Roy, R. R. Dighe, A. R. Chakravarty, *Inorg. Chem.*, 48, (2009) 2652.
41. S. Li, K. Huang, M. Zhong, J. Guo, W. Z. Wang, R. Zhu, *Spectrochim. Acta, Part A*, 77, (2010) 680.
42. A. J. Sulkowska, *J. Mol. Struct.*, 614, (2002) 227.
43. Y. J. Hu, Y. Liu, L. X. Zhang, R. M. Zhao, S. S. Qu, *J. Mol. Struct.*, 750, (2002) 174..
44. B. P. Kamat, J. Seetharamappa, *Journal Photosci.*, 11, (2004) 29.
45. Y. Z. Zhang, B. Zhou, Y. X. Liu, C. X. Zhou, X. L. Ding, Y. Liu, *J. Fluoresc.*, 18, (2008) 109.
46. S. Anbu, M. Kandaswamy, P. Suthakaran, V. Murugan, B. Varghese, *Inorg. Biochem.*, 103, (2009).
47. C. Q. Jiang, M. X. Gao, J. X. He, *Anal. Chim. Acta.*, 452, (2002) 185.
48. H. Ojha, K. Mishra, M. Hassan, N. K. Chaudhary, *Thermochim. Acta.*, 548, (2012) 56.

Figure Captions

Fig. 1. Some triazole based market available drugs

Scheme 1. Preparation of the ligands $\mathbf{H}_2\mathbf{L}^1$, $\mathbf{H}_2\mathbf{L}^2$ and their metal complexes **1–8**

Fig. 2. Mass Spectrum of metal complex **2**

Fig. 3. ^1H NMR spectra of ligand $\mathbf{H}_2\mathbf{L}^1$

Fig. 4. Thermogravimetric curves of metal complexes **(1)** $[\text{Co}(\text{L}^1)(\text{H}_2\text{O})_3]$; **(2)** $[\text{Ni}(\text{L}^1)(\text{H}_2\text{O})_3]$; **(3)** $[\text{Cu}(\text{L}^1)(\text{H}_2\text{O})]$; **(4)** $[\text{Zn}(\text{L}^1)(\text{H}_2\text{O})]$

Fig. 5. Fluorescence quenching spectra of BSA at different concentrations of complexes **1(a)**, **2(b)**, **3(c)**, **4(d)**; $[\text{BSA}] = 15 \mu\text{M}$; $[\text{Complex 1–4}]$ varied from 6.62–32.2 μM .

Fig. 6. Stern–Volmer Plot F_0/F versus $[\text{Q}]$ for the Binding of BSA with metal complexes **1–4**

Fig. 7. Stern–Volmer Plot $\log [F_0 - F / F]$ versus $\log [\text{Q}]$ for the Binding of BSA with metal complexes **1–4**

Fig. 8. Geometry Optimized structures of (a) Ligand $\mathbf{H}_2\mathbf{L}^1$, (b) Complex **1**, (c) Complex **2**, (d) Complex **3**, **(e)** Complex **4** (Colour Code: H=White, C=Grey, N= Blue, O=red, Co= Grey, Ni= Silver Grey, Cu=Pink, Zn=grey)

Scheme 2. : Numbering Scheme of the optimized structures (a) Ligand $\mathbf{H}_2\mathbf{L}^1$, (b) Complexes **1–2**; **5–6** (c) **3–4**; **7–8**

Fig. 9. Proposed Structure of the newly obtained metal complexes

Fig. 10. Ligand $\mathbf{H}_2\mathbf{L}^1$, $\mathbf{H}_2\mathbf{L}^2$ and metal complexes (**1–8**) inhibited the cell viability of HepG2 & MCF-7 cells (Data were assayed by ANOVA and Student's *t*-test. Differences between means were considered significant when yielding a $P < 0.05$. Results are presented as means \pm S.D.

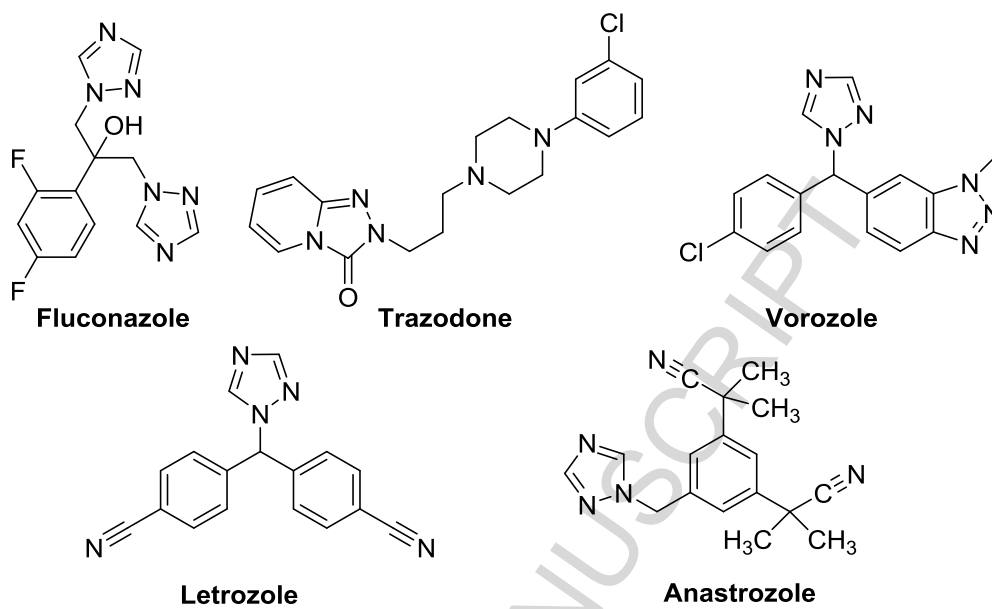


Fig. 1. Some triazole based market available drugs

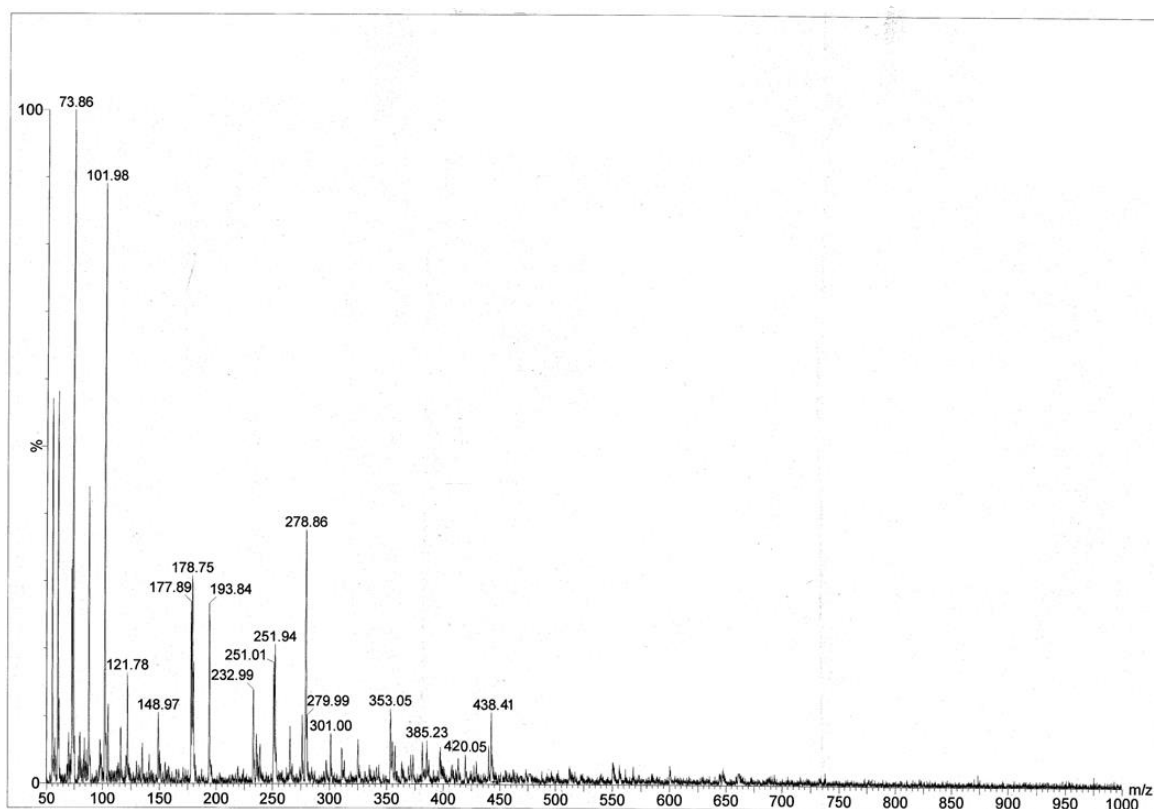


Fig. 2. Mass Spectrum of metal complex 1

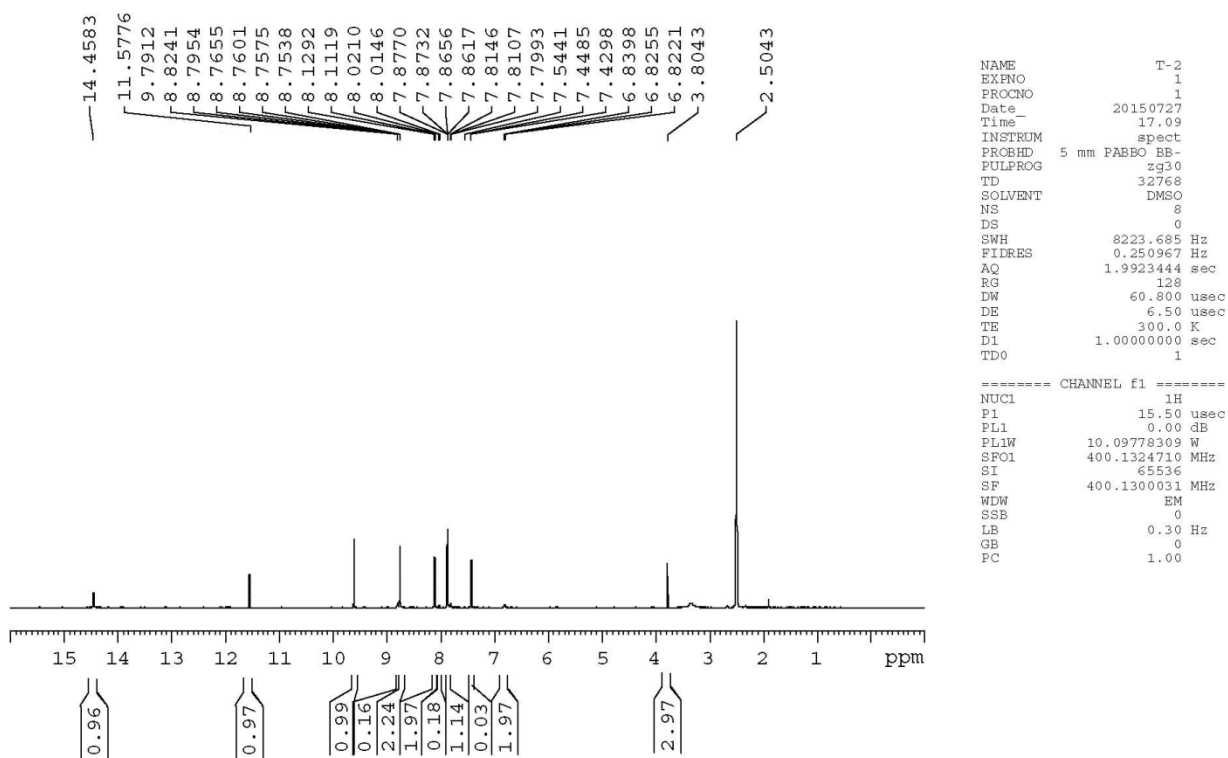


Fig. 3. ^1H NMR spectra of ligand H_2L^1

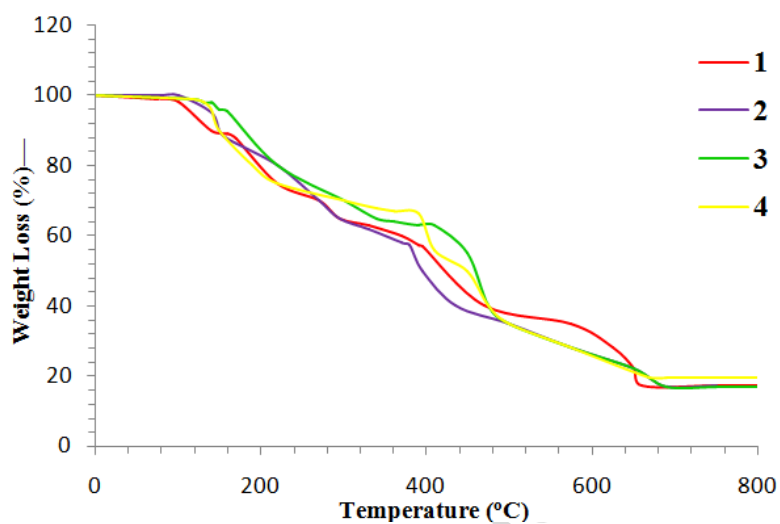


Fig. 4. Thermogravimetric curves of metal complexes (1) $[\text{Co}(\text{L}^1)(\text{H}_2\text{O})_3]$; (2) $[\text{Ni}(\text{L}^1)(\text{H}_2\text{O})_3]$; (3) $[\text{Cu}(\text{L}^1)(\text{H}_2\text{O})]$; (4) $[\text{Zn}(\text{L}^1)(\text{H}_2\text{O})]$

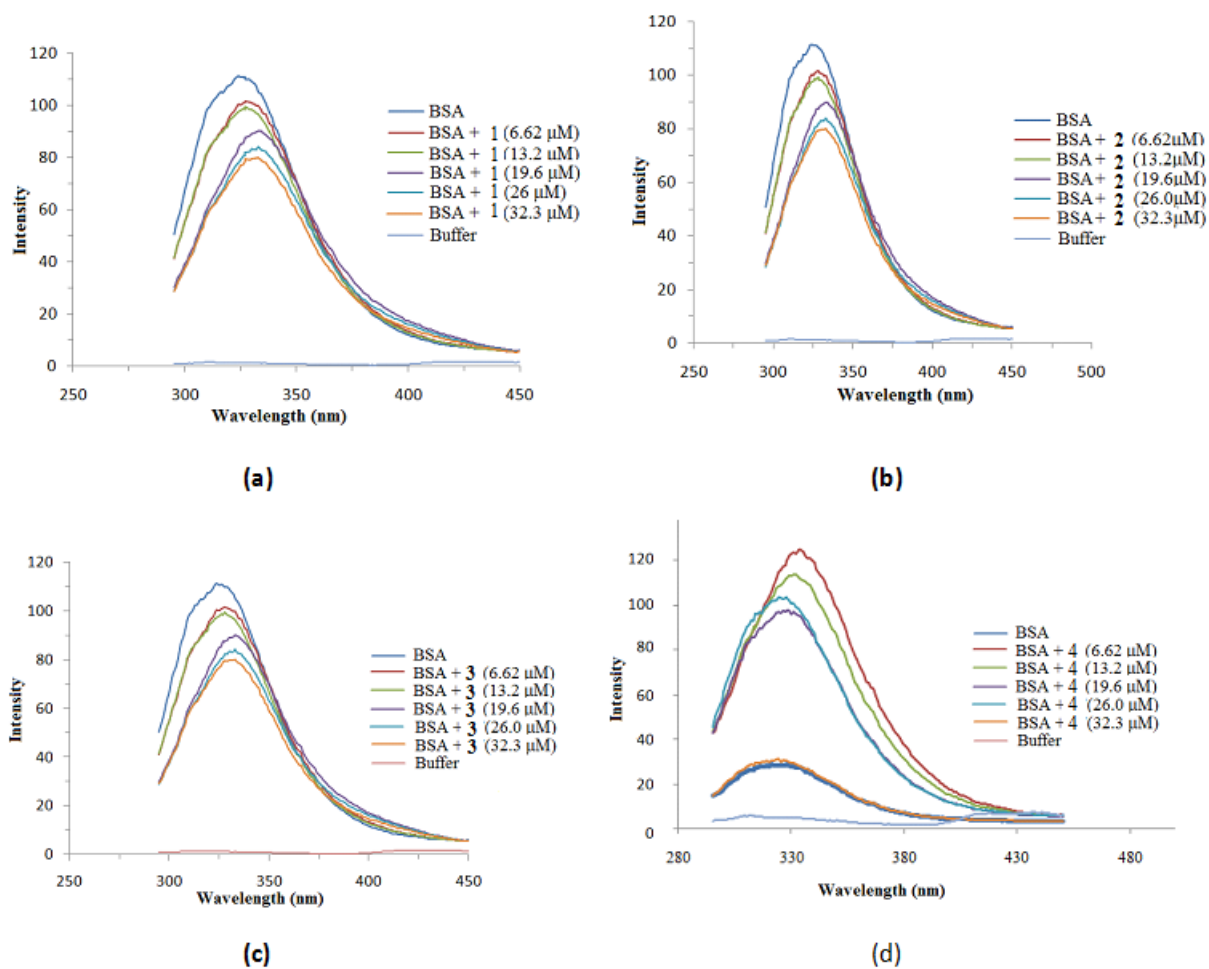


Fig. 5. Fluorescence quenching spectra of BSA at different concentrations of complexes 1(a), 2(b), 3(c), 4(d); [BSA] = 15 μM ; [Complex 1–4] varied from 6.62–32.2 μM .

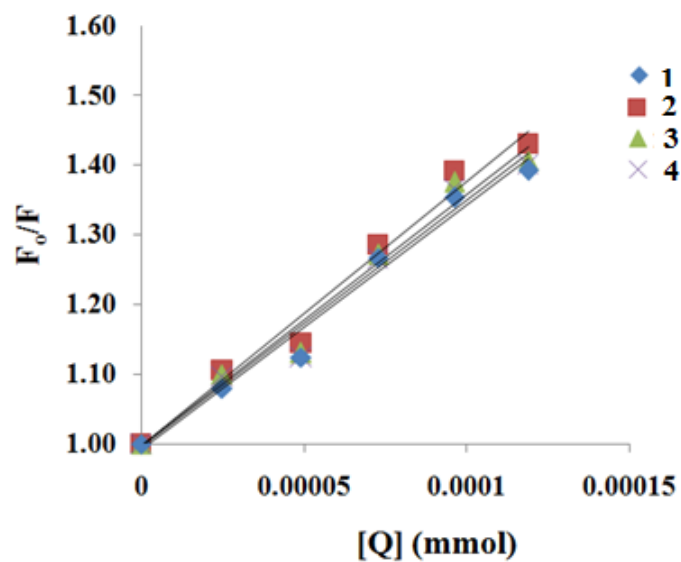


Fig. 6: Stern–Volmer Plot F_0/F versus $[Q]$ for the Binding of BSA with metal complexes 1–4

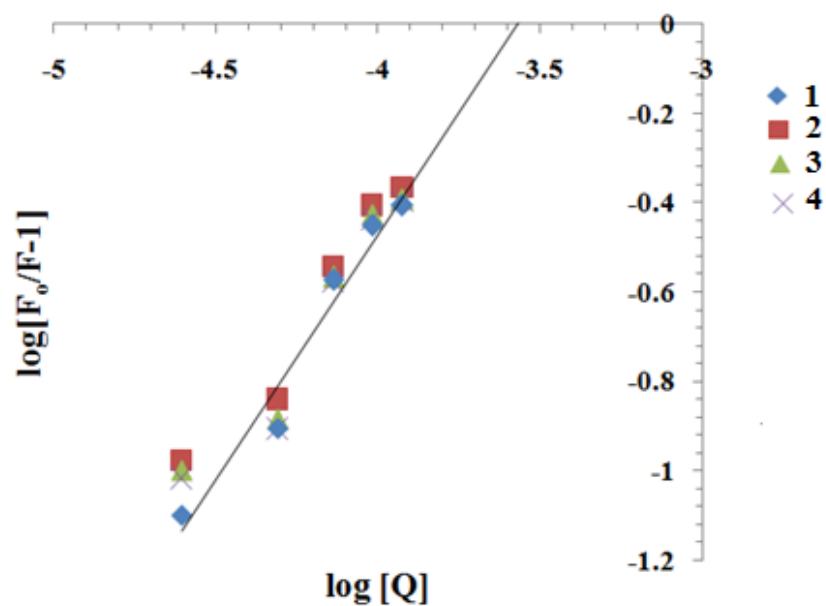


Fig. 7 : Stern–Volmer Plot $\log [F_0-F /F]$ versus $\log [Q]$ for the Binding of BSA with metal complexes 1–4

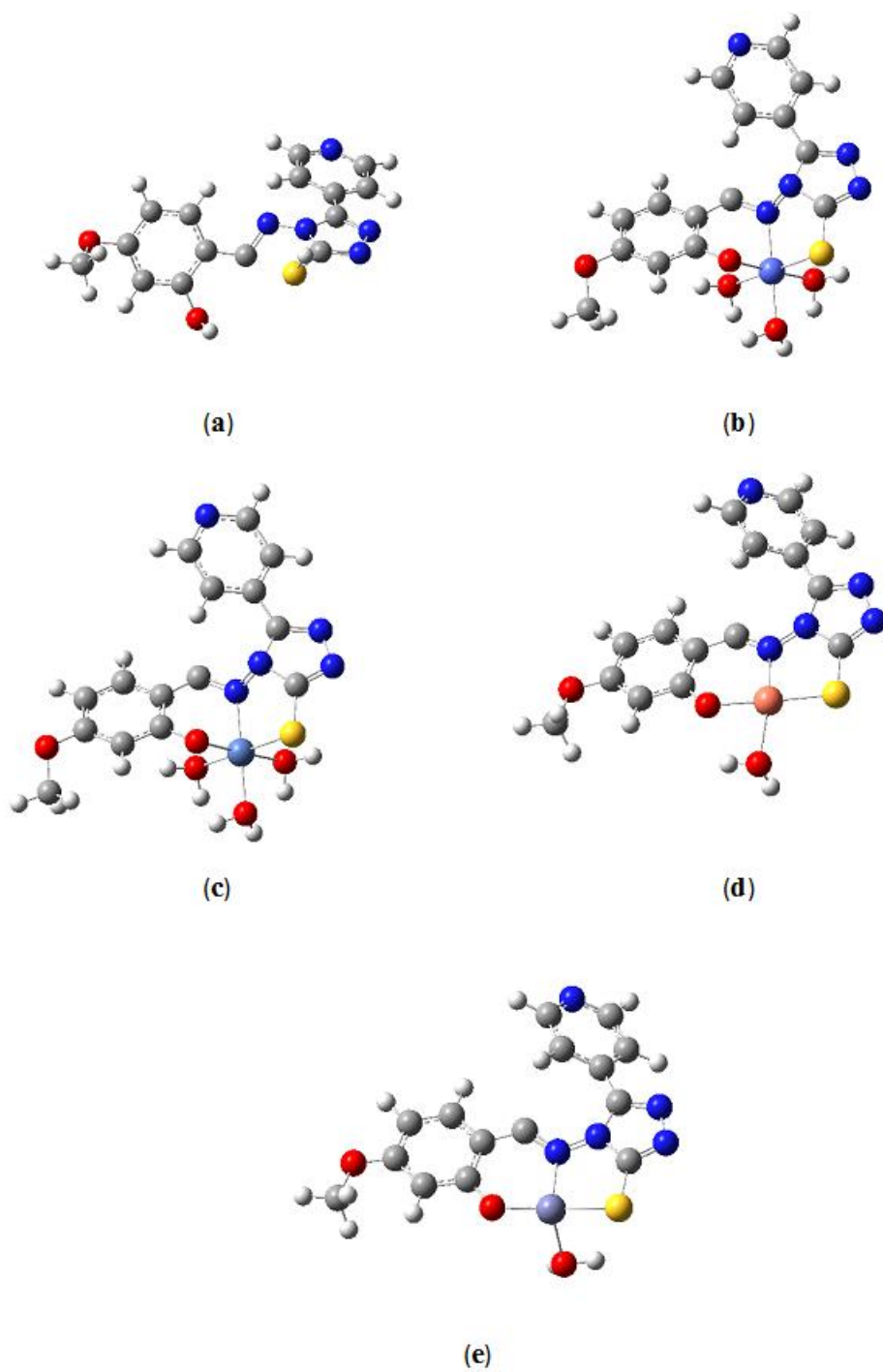


Fig. 8. Geometry Optimized structures of (a) Ligand H_2L^1 , (b) Complex **1**, (c) Complex **2**, (d) Complex **3**, (e) Complex **4** (Colour Code: H=White, C=Grey, N= Blue, O=red, Co= Grey, Ni= Silver Grey, Cu=Pink, Zn=grey)

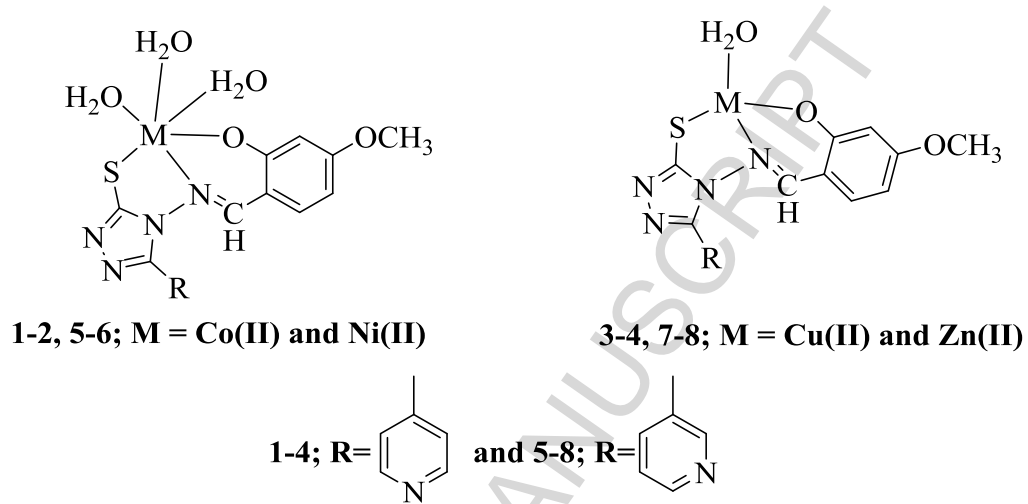


Fig. 9. Proposed Structure of the newly obtained metal complexes

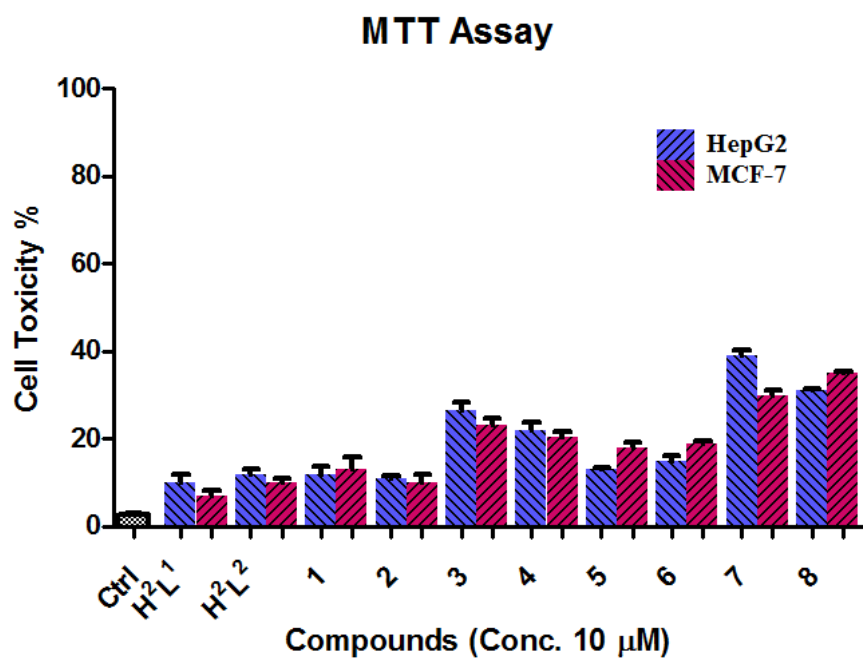
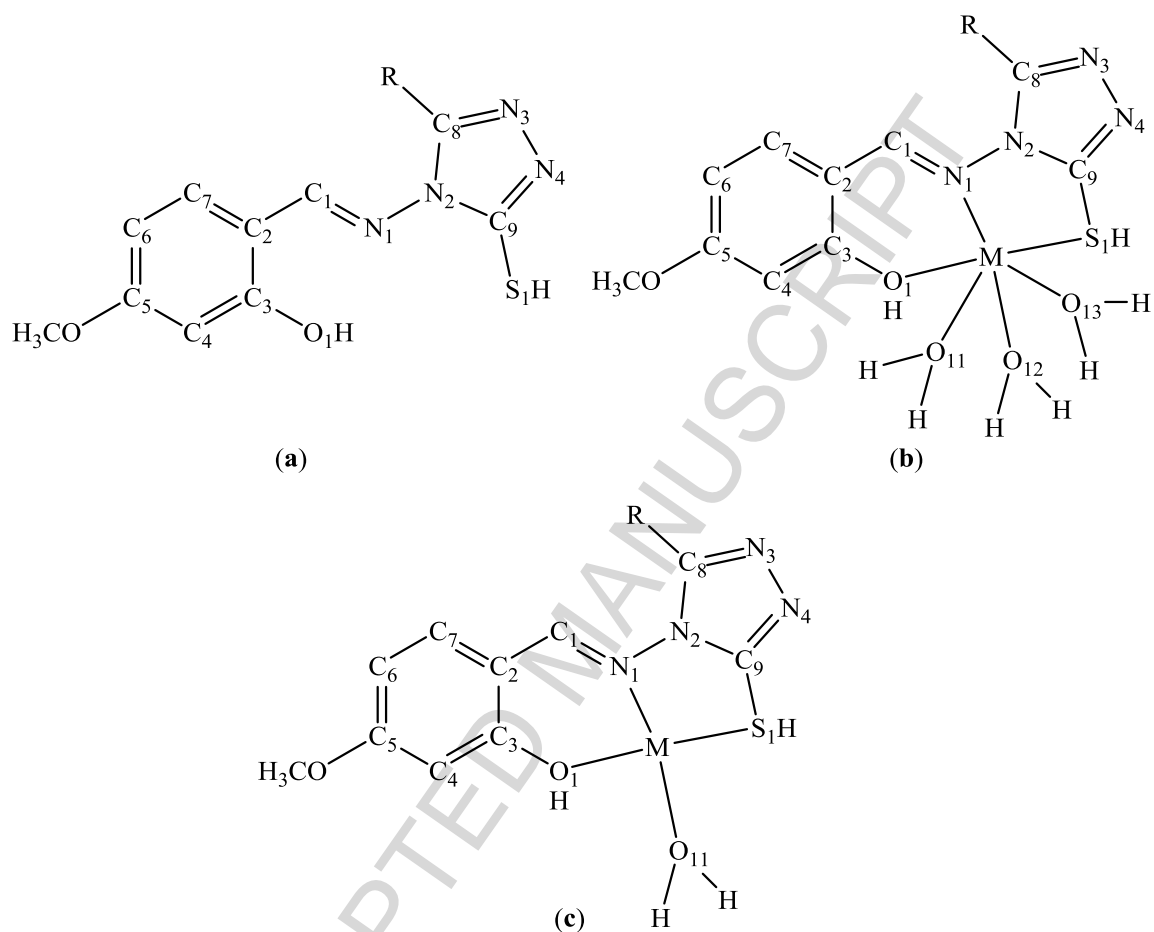


Fig. 10. % Cell toxicity of Ligand H₂L¹, H₂L² and metal complexes (1–8) against cell line HepG2 & MCF-7 (Data were assayed by ANOVA and Student's *t*-test. Differences between means were considered significant when yielding a $P < 0.05$. Results are presented as means \pm S.D.



Scheme 2. : Numbering Scheme of the optimized structures (a) Ligand $\mathbf{H}_2\mathbf{L}^1$, (b) Complexes 1–2; 5–6 (c) 3–4; 7–8

Table 1: Physical measurements and analytical data of the ligand ($\mathbf{H}_2\mathbf{L}^1$, $\mathbf{H}_2\mathbf{L}^2$) and metal complexes(**1-8**).

No.	Molecular mass/ molecular formula	m/z	Yield (%)	Elemental Analysis (%) found			
				(calc.)			
				C	H	N	M ^a
$\mathbf{H}_2\mathbf{L}^1$	$\text{C}_{15}\text{H}_{13}\text{N}_5\text{O}_2\text{S}$ [327.36]	328.01	74	55.00 (55.04)	4.02 (4.00)	21.35 (21.39)	-
$\mathbf{H}_2\mathbf{L}^2$	$\text{C}_{15}\text{H}_{13}\text{N}_5\text{O}_2\text{S}$ [327.36]	328.13	69	55.12 (55.04)	3.98 (4.00)	21.36 (21.39)	-
1	$[\text{Co}(\text{L}^1)(\text{H}_2\text{O})_3]$ [438.03] $\text{C}_{15}\text{H}_{17}\text{CoN}_5\text{O}_5\text{S}$	438.41	60	41.15 (41.10)	3.95 (3.91)	16.04 (15.98)	13.39 (13.45)
2	$[\text{Ni}(\text{L}^1)(\text{H}_2\text{O})_3]$ [437.03] $\text{C}_{15}\text{H}_{17}\text{N}_5\text{NiO}_5\text{S}$	437.30	58	41.09 (41.13)	3.91 (3.91)	16.03 (15.99)	13.45 (13.40)
3	$[\text{Cu}(\text{L}^1)(\text{H}_2\text{O})]$ [406.0] $\text{C}_{15}\text{H}_{13}\text{CuN}_5\text{O}_3\text{S}$	406.71	65	44.25 (44.28)	3.21 (3.22)	17.25 (17.21)	15.55 (15.62)
4	$[\text{Zn}(\text{L}^1)(\text{H}_2\text{O})]$ [407.0] $\text{C}_{15}\text{H}_{13}\text{N}_5\text{O}_3\text{SZn}$	407.18	72	44.15 (44.08)	3.35 (3.21)	17.13 (17.13)	16.04 (16.00)
5	$[\text{Co}(\text{L}^2)(\text{H}_2\text{O})_3]$ [438.03] $\text{C}_{15}\text{H}_{17}\text{CoN}_5\text{O}_5\text{S}$	438.26	53	41.12 (41.10)	3.97 (3.91)	16.01 (15.98)	13.44 (13.45)
6	$[\text{Ni}(\text{L}^2)(\text{H}_2\text{O})_3]$ [437.03] $\text{C}_{15}\text{H}_{17}\text{N}_5\text{NiO}_5\text{S}$	437.63	58	41.15 (41.13)	3.96 (3.91)	15.95 (15.99)	13.41 (13.40)
7	$[\text{Cu}(\text{L}^2)(\text{H}_2\text{O})]$ [406.0] $\text{C}_{15}\text{H}_{13}\text{CuN}_5\text{O}_3\text{S}$	406.80	62	44.27 (44.28)	3.25 (3.22)	17.29 (17.21)	15.70 (15.62)
8	$[\text{Zn}(\text{L}^2)(\text{H}_2\text{O})]$ [407.0] $\text{C}_{15}\text{H}_{13}\text{N}_5\text{O}_3\text{SZn}$	407.81	66	44.15 (44.08)	3.36 (3.21)	17.22 (17.13)	16.01 (16.00)

^a M = Co(II), Ni(II), Cu(II), Zn(II)

Table 2: Important infrared spectral bands (cm^{-1}) and their assignments

Compound	$\nu(\text{HC}=\text{N})$	$\nu(-\text{OH})$	$\nu(-\text{SH})$	$\nu(\text{M}-\text{O})$	$\nu(\text{M}-\text{N})$	$\nu(\text{M}-\text{S})$
H_2L^1	1598	3230	2704	-	-	-
H_2L^2	1601	3213	2698	-	-	-
1	1586	-	-	532	434	342
2	1682	-	-	530	423	356
3	1579	-	-	522	449	354
4	1581	-	-	531	435	366
5	1585	-	-	515	449	351
6	1586	-	-	512	432	355
7	1579	-	-	510	430	366
8	1582	-	-	519	437	349

Table 3: Conductivity, magnetic and electronic spectra of metal complexes **1–8**

No.	Ω_M ($\Omega^{-1}\text{cm}^2\text{mol}^{-1}$)	B.M (μ_{eff})	$1/\lambda(\text{cm}^{-1})$
1	7.2	4.98	10749, 19668
2	5.4	2.94	11044, 15656, 24125
3	8.6	1.81	20012
4	11.6	-	-
5	10.2	5.03	10112, 19998
6	7.9	2.98	10713, 16415, 25675
7	11.6	1.83	18978
8	9.8	-	-

Table 4: Thermal Analysis data of metal complexes (1–4).

Comp. No	Molecular Formula	Stages	Temp (°C)	Possible Evolved Species	Residual Mass Loss (%)		
					Species	Found	Calc.
1	[Co(L ¹)(H ₂ O) ₃] [438.03]	1 st	140–170	3H ₂ O		12.34	12.32
	C ₁₅ H ₁₇ CoN ₅ O ₅ S	2 nd	170–390	C ₈ H ₇ NO		30.28	30.37
		3 rd	390–660	triazole moiety		40.24	40.20
					CoO	17.10	17.12
2	[Ni(L ¹)(H ₂ O) ₃] [437.03]	1 st	140–160	3H ₂ O		12.31	12.35
	C ₁₅ H ₁₇ N ₅ NiO ₅ S	2 nd	160–370	C ₈ H ₇ O		27.29	27.24
		3 rd	370–690	triazole moiety		43.32	43.50
					NiO	16.88	16.93
3	[Cu(L ¹)(H ₂ O)] [406.0]	1 st	130–160	H ₂ O		4.45	4.43
	C ₁₅ H ₁₃ CuN ₅ O ₃ S	2 nd	160–410	C ₈ H ₇ NO		32.83	32.77
		3 rd	410–700	triazole moiety		43.30	43.37
					CuO	19.62	19.46
4	[Zn(L ¹)(H ₂ O)] [407.0]	1 st	140–390	C ₈ H ₉ O ₂		33.62	33.67
	C ₁₅ H ₁₃ N ₅ O ₃ SZn	2 nd	390 – 670	triazole moiety		46.75	46.71
					ZnO	19.55	19.66

Table 5: Bonding coefficient parameters of copper complexes

Complex	g_{\parallel}	g_{\perp}	K_{\parallel}	K_{\perp}	α	β	β_1	G
3 [Cu(L ¹)(H ₂ O)]	2.148	2.067	0.66	0.72	0.66	1.09	1	2.20
7 [Cu(L ²)(H ₂ O)]	2.241	2.074	0.82	0.74	0.82	0.90	1	3.25

Table 6: Stern-Volmer constant and bimolecular quenching rate constant for metal complexes **1–4**.

No.	K_{sv} (mol^{-1})	K_q ($\text{mol}^{-1}\text{sec}^{-1}$)	R^2
1	3.782×10^3	3.782×10^{12}	0.978
2	3.597×10^3	3.597×10^{12}	0.972
3	3.534×10^3	3.534×10^{12}	0.995
4	3.504×10^3	3.504×10^{12}	0.977

Table 7: Binding constant and number of binding site for metal complexes **1–4**.

No	K_b	n	R^2
1	2.97×10^3	0.996	0.946
2	2.94×10^3	0.983	0.929
3	3.38×10^3	0.999	0.926
4	8.22×10^3	1.09	0.960

Table 8: Optimized geometry of the ligand H_2L^1 and metal complexes **1–3** (bond lengths in Angstroms; bond angles in degrees).

Parameters ^a	Ligand H_2L^1	Complex 1 ^b	Complex 2 ^c	Complex 3 ^d	Complex 4 ^e
C ₁ – C ₂	1.495	1.497	1.499	1.388	1.394
C ₂ – C ₃	1.485	1.514	1.526	1.463	1.443
C ₃ – C ₄	1.474	1.485	1.487	1.417	1.403
C ₄ – C ₅	1.480	1.482	1.485	1.391	1.382
C ₅ – C ₆	1.480	1.480	1.481	1.419	1.406
C ₆ – C ₇	1.476	1.475	1.473	1.371	1.364
C ₇ – C ₂	1.488	1.489	1.490	1.388	1.414
C ₃ – O ₁	1.464	1.468	1.469	1.298	1.302
C ₁ – N ₁	1.427	1.439	1.437	1.253	1.270
N ₁ – N ₂	1.442	1.455	1.466	1.378	1.364
N ₂ – C ₈	1.452	1.453	1.482	1.395	1.379
N ₂ – C ₉	1.454	1.472	1.486	1.385	1.381
C ₉ – S ₁	1.787	1.788	1.787	1.734	1.737
M – O ₁	-	2.089	2.091	1.951	1.864
M – N ₁	-	2.074	2.076	2.010	2.018
M – S ₁	-	2.384	2.393	2.212	2.239
M – O ₁₁	-	2.134	2.135	2.185	2.100
M – O ₁₂	-	2.118	2.124	-	-
M – O ₁₃	-	2.121	2.123	-	-
∠N ₁ M□ ₁	-	85.46	86.16	92.89	96.20
∠S ₁ MN ₁	-	86.12	87.19	90.04	91.39
∠O ₁ MO ₁₁	-	87.23	85.34	79.14	104.94
∠O ₁ MS ₁	-	94.12	92.59	172.96	-
∠O ₁₁ MO ₁₂	-	88.17	90.92	79.27	-
∠N ₁ MO ₁₂	-	178.12	186.19	-	-

^a Scheme 2 for numbering^b M=Co, ^c M=Ni, ^d M=Cu, ^e M=Zn

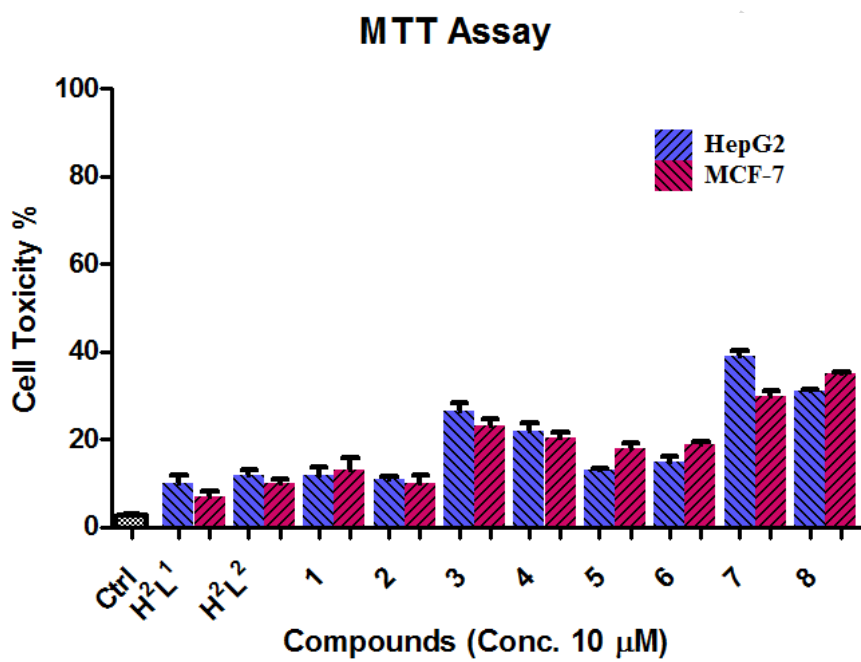
Table 9: Effect of a ligands H_2L^1 , H_2L^2 and series of metal complexes (1–8) at two concentrations of 5 and 10 μM on the HepG2 and MCF-7 cell proliferation.^a

Compound	Survival cell		Cell growth		Survival cell		Cell growth	
	fraction (%) at 5 μM		inhibition (%) at 5 μM		fraction (%) at 10 μM		inhibition (%) at 10 μM	
	HepG2	MCF-7	HepG2	MCF-7	HepG2	MCF-7	HepG2	MCF-7
Control	100 \pm 2	100 \pm 1	-	-	100 \pm 1	100 \pm 2	-	-
H_2L^1	92 \pm 3	95 \pm 4	8	5	90 \pm 3	93 \pm 2	10	7
H_2L^2	90 \pm 4	91 \pm 3	10	9	88 \pm 2	90 \pm 1	12	10
1	89 \pm 4	91 \pm 4	11	9	88 \pm 3	87 \pm 4	12	13
2	91 \pm 3	93 \pm 3	9	7	89 \pm 1	90 \pm 3	11	10
3	88 \pm 5	89 \pm 3	12	11	74 \pm 3	78 \pm 2	26	22 ^b
4	87 \pm 3	86 \pm 3	13	14	78 \pm 4	81 \pm 2	22	19
5	90 \pm 3	90 \pm 4	10	10	87 \pm 2	82 \pm 3	13	18 ^b
6	88 \pm 5	89 \pm 1	12	11	85 \pm 1	81 \pm 2	15	19 ^b
7	80 \pm 3	82 \pm 2	20	18	61 \pm 2	70 \pm 2	39	30
8	85 \pm 2	81 \pm 3	15	19	69 \pm 1	65 \pm 1	31 ^b	35

^a The results are expressed as the percentage of viable cells with respect to the control and are presented as mean \pm SD.

^b Significantly different from the control

Graphical abstract



% Cell toxicity of Ligand H₂L¹, H₂L² and metal complexes (1–8) against cell line HepG2 & MCF-7

Highlights

- 1,2,4-triazole derived novel Schiff bases
- Co(II), Ni(II), Cu(II) and Zn(II) complexes
- Thermogravimetric analysis
- DFT calculation
- BSA binding fluorescence study
- *In vitro* anticancer cell line activity.

ACCEPTED MANUSCRIPT